

Status of the two-Higgs-doublet model in light of the CDF m_W measurement

Soojin Lee,^{1,*} Kingman Cheung,^{1,2,3,†} Jinheung
Kim,^{1,‡} Chih-Ting Lu,^{4,§} and Jeonghyeon Song^{1,¶}

¹*Department of Physics, Konkuk University, Seoul 05029, Republic of Korea*

²*Department of Physics, National Tsing Hua University, Hsinchu 300, Taiwan*

³*Center for Theory and Computation,*

National Tsing Hua University, Hsinchu 300, Taiwan

⁴*Department of Physics and Institute of Theoretical Physics,*

Nanjing Normal University, Nanjing, 210023, China

Abstract

The most recent the W -boson mass measurement by the CDF Collaboration with a substantially reduced uncertainty indicated a large deviation from the standard model prediction, as large as 7σ if taken literally. In terms of the Peskin-Takeuchi parameters of S and T , the central values would shift to larger values. It has profound consequences in searching for physics beyond the SM. We show in the framework of two-Higgs-doublet Models the effect of the new m_W^{CDF} measurement on the parameter space. Combined this m_W^{CDF} measurement with other constraints including theoretical requirements, flavor-changing neutral currents in B physics, maintaining the perturbativity of all couplings until the cutoff scale $\Lambda_c = 1$ TeV, Higgs precision data, and direct collider search limits from the LEP, Tevatron, and LHC experiments, we find upper bounds on the masses of the heavy Higgs bosons $M_{H,A,H^\pm} \lesssim 1000 - 1100$ GeV in type-I, II, X, and Y for the normal scenario and $M_{H^\pm,A} \lesssim 410 - 440$ GeV in type I and X for the inverted scenario. Another important finding is that type-II and type-Y in the inverted scenario are completely excluded. Such unprecedented findings imply that the upcoming LHC run can readily close out the still-available parameter space.

Keywords: Higgs Physics, Beyond the Standard Model, electroweak precision data

*Electronic address: soojinlee957@gmail.com

†Electronic address: cheung@phys.nthu.edu.tw

‡Electronic address: jinheung.kim1216@gmail.com

§Electronic address: timluyu@gmail.com

¶Electronic address: jhsong@konkuk.ac.kr

Contents

I. Introduction	2
II. Review of 2HDM	4
III. Scanning strategies	7
IV. Characteristic features of the normal scenario	11
A. type-I and type-X	12
B. type-II and type-Y	16
V. Characteristic features of the inverted scenario	17
VI. Conclusions	18
Acknowledgments	20
References	20

I. INTRODUCTION

The standard model (SM) of electroweak theory with $SU(2) \times U(1)$ gauge symmetry is highly successful in explaining almost all the observations in particle physics experiments, especially after discovering the final piece of SM, the Higgs boson. Therefore, we believe that the SM is at least a good effective theory for the energy scale below TeV. On the other hand, theorists have not stopped extending the SM to answer the outstanding questions in particle physics, such as the neutrino mass and mixing, matter-antimatter asymmetry in the Universe and dark matter. Hence, if any experiment at the energy scale below about 1 TeV observes an anomaly, it would shake the foundation of the SM.

Very recently, the CDF collaboration at Fermilab reported the most precise W boson mass measurement: $m_W^{\text{CDF}} = 80.4335 \pm 0.0094$ GeV [1]. The total uncertainty is less than 10 MeV and the central value is about 76.5 MeV larger than the SM prediction: $m_W^{\text{SM}} = 80.357 \pm 0.006$ GeV [2]). We have about 7σ standard deviation from the SM prediction. Before the CDF run-II result, the world average of m_W measurements was just 1.8σ standard deviation from the SM expectation [2]. Even though more careful cross-checks of the systematic uncertainties among CDF run-II analysis and other W boson mass measurements such as LEP [3], LHCb [4], ATLAS [5], and D0 [6] are still needed, the validity of the SM is questioned and possible explanations from new physics models are pursued after this new measured m_W value.

The global fit to the electroweak precision data (EWPD) is one of the most powerful tools to quantify the consistency of the SM and point in the direction of new physics [7, 8]. Therefore, the new global electroweak fit should be the first step to approaching this W boson mass anomaly.

According to Ref. [9–19], it is hard to explain m_W^{CDF} without going beyond the SM. An efficient way to parametrize the impact of new physics on the global EW fits is a set of Peskin-Takeuchi oblique parameters S , T , and U [20–22]. If all of these three parameters can vary, the new fits show that S and T can keep as before, but the U increases substantially such that $S = 0.06 \pm 0.10$, $T = 0.11 \pm 0.12$, $U = 0.13 \pm 0.09$ [9]. However, the contributions to U can only appear in the dimension-eight operator and most new physics models have tiny contributions to U . Therefore, setting $U = 0$ while varying S and T is reassumed, resulting in both S and T moving to large and positive values: $S = 0.14 \pm 0.08$ and $T = 0.26 \pm 0.06$ [9]. Based on these changes of S and T , some new physics models including two-Higgs-doublet model (2HDM) and its extensions [9, 23–34], the Higgs triplet model [35–39], supersymmetry [40–45], leptoquarks [46–48], seesaw mechanisms of neutrino mass and their extensions [49–53], vector-like leptons or vector-like quarks [54–57], the standard model effective field theory (SMEFT) [11–14, 16, 17, 58–60], and others [10, 18, 19, 61–69] are proposed to explain this W boson mass anomaly. Especially, some of them also try to explain the long-standing tension in muon $g - 2$ measurement [32, 33, 41, 42, 46–48, 52, 54, 55, 57] which has been confirmed from Fermilab [70].

In this work, we pursue a comprehensive study of the 2HDM in light of the new CDF m_W measurement. We study not only four famous tree-level flavor-conserved types (type-I, type-II, type-X, and type-Y) but also two scenarios for the observed Higgs boson, the normal scenario (NS) and inverted scenario (IS). We impose all the theoretical and experimental constraints, including the stability of the scalar potential, the electroweak precision data (EWPD) with the new CDF m_W measurement, the Higgs precision data, and the direct search bounds for new scalar bosons at the LEP, Tevatron, and LHC. In addition, we study the RGE evolutions of the model parameters, and demand the stability of the 2HDM potential up to 1 TeV, i.e., the cutoff scale Λ_c above 1 TeV. Combining $\Lambda_c > 1$ TeV with the other constraints puts the upper bounds on the masses of new Higgs bosons at about 1 TeV. The upper bound on the charged Higgs boson mass by $\Lambda_c > 1$ TeV causes a conflict with the lower bound on M_{H^\pm} from $b \rightarrow s\gamma$ [71, 72] for type-II and type-Y, especially in the IS. Consequently, type-II and type-Y in the IS are excluded in light of the CDF m_W measurement. This is one of the most salient results in our paper. A total of eight cases, four types in the NS and IS, are thoroughly investigated by scanning the whole parameter space without any conditions on the masses and couplings. And the results give apparent signals for the future collider phenomenologies: (i) type-I has the most survival parameter points for both NS and IS; (ii) the light charged Higgs boson with mass below the top quark mass is viable in type-I of the NS; (iii) light neutral Higgs bosons, CP -even and CP -odd, are still allowed for type-I and type-X.

The rest of this paper is arranged as follows. We first briefly review the 2HDM in Sec. II. The parameter scanning strategies are introduced in Sec. III, and the allowed mass ranges of new Higgs bosons are also shown. We then discuss the characteristic features of the normal and inverted scenarios of 2HDMs in Sec. IV and Sec. V, respectively. Finally, we conclude in Sec. VI.

II. REVIEW OF 2HDM

In the 2HDM, there exist two complex $SU(2)_L$ Higgs scalar doublet fields, Φ_1 and Φ_2 [73]:

$$\Phi_i = \begin{pmatrix} w_i^+ \\ \frac{v_i + h_i + i\eta_i}{\sqrt{2}} \end{pmatrix}, \quad i = 1, 2, \quad (1)$$

where v_1 and v_2 are the nonzero vacuum expectation values of Φ_1 and Φ_2 , respectively. The electroweak symmetry is broken by $v = \sqrt{v_1^2 + v_2^2} = 246$ GeV. We define the ratio of two vacuum expectation values to be $\tan\beta = v_2/v_1$. For simplicity, we use the simplified notation of $s_x = \sin x$, $c_x = \cos x$, and $t_x = \tan x$ ($x = \beta, \beta - \alpha, \dots$) in what follows.

We additionally impose a discrete Z_2 symmetry, under which $\Phi_1 \rightarrow \Phi_1$ and $\Phi_2 \rightarrow -\Phi_2$, to avoid the flavor-changing-neutral-current (FCNC) at tree level [74, 75]. The scalar potential with softly broken Z_2 and CP invariance is

$$\begin{aligned} V = & m_{11}^2 \Phi_1^\dagger \Phi_1 + m_{22}^2 \Phi_2^\dagger \Phi_2 - m_{12}^2 (\Phi_1^\dagger \Phi_2 + \text{H.c.}) \\ & + \frac{1}{2} \lambda_1 (\Phi_1^\dagger \Phi_1)^2 + \frac{1}{2} \lambda_2 (\Phi_2^\dagger \Phi_2)^2 + \lambda_3 (\Phi_1^\dagger \Phi_1) (\Phi_2^\dagger \Phi_2) + \lambda_4 (\Phi_1^\dagger \Phi_2) (\Phi_2^\dagger \Phi_1) \\ & + \frac{1}{2} \lambda_5 \left[(\Phi_1^\dagger \Phi_2)^2 + \text{H.c.} \right], \end{aligned} \quad (2)$$

where the m_{12}^2 term softly breaks the Z_2 parity. The model has five physical Higgs bosons, the lighter CP -even scalar h , the heavier CP -even scalar H , the CP -odd pseudoscalar A , and a pair of charged Higgs bosons H^\pm . The weak eigenstates in Eq. (1) are linear combinations of physical Higgs bosons through two mixing angles α and β , which are referred to Ref. [76]. A significant relation is the SM Higgs boson h_{SM} with h and H :

$$h_{\text{SM}} = s_{\beta-\alpha} h + c_{\beta-\alpha} H. \quad (3)$$

In the 2HDM, the observed Higgs boson at a mass of 125 GeV can be either h or H , which is called the normal scenario (NS) and the inverted scenario (IS), respectively:

$$\text{NS: } m_h = m_{125}; \quad (4)$$

$$\text{IS: } M_H = m_{125},$$

where m_{125} is the observed Higgs boson mass. For the consistency with the Higgs precision data at the LHC, the Higgs alignment limit has drawn a lot of attention, where $h = h_{\text{SM}}$ in the NS and $H = h_{\text{SM}}$ in the IS. Even though the limit simplifies the phenomenology of the new Higgs bosons such that $H \rightarrow WW/ZZ$, $A \rightarrow Zh$, and $H^\pm \rightarrow W^{\pm(*)}h$ are prohibited at tree level, it may interfere with the observation of the 2HDM. Therefore, we pursue the allowed parameter space without any conditions on the masses and couplings. Only the theoretical and experimental constraints will be taken into account to restrict the parameter space.

We take the physical parameter basis of

$$\{m_h, M_{H^\pm}, M_H, M_A, m_{12}^2, t_\beta, s_{\beta-\alpha}\}, \quad (5)$$

	ξ_{Su}^h	ξ_{Sd}^h	$\xi_{S\ell}^h$	ξ_{Su}^H	ξ_{Sd}^H	$\xi_{S\ell}^H$	ξ_{Su}^A	ξ_{Sd}^A	$\xi_{S\ell}^A$
Type-I	$\frac{c_\alpha}{s_\beta}$	$\frac{c_\alpha}{s_\beta}$	$\frac{c_\alpha}{s_\beta}$	$\frac{s_\alpha}{s_\beta}$	$\frac{s_\alpha}{s_\beta}$	$\frac{s_\alpha}{s_\beta}$	$\frac{1}{t_\beta}$	$-\frac{1}{t_\beta}$	$-\frac{1}{t_\beta}$
Type-II	$\frac{c_\alpha}{s_\beta}$	$-\frac{s_\alpha}{c_\beta}$	$-\frac{s_\alpha}{c_\beta}$	$\frac{s_\alpha}{s_\beta}$	$\frac{c_\alpha}{c_\beta}$	$\frac{c_\alpha}{c_\beta}$	$\frac{1}{t_\beta}$	t_β	t_β
Type-X	$\frac{c_\alpha}{s_\beta}$	$\frac{c_\alpha}{s_\beta}$	$-\frac{s_\alpha}{c_\beta}$	$\frac{s_\alpha}{s_\beta}$	$\frac{s_\alpha}{s_\beta}$	$\frac{c_\alpha}{c_\beta}$	$\frac{1}{t_\beta}$	$-\frac{1}{t_\beta}$	t_β
Type-Y	$\frac{c_\alpha}{s_\beta}$	$-\frac{s_\alpha}{c_\beta}$	$\frac{c_\alpha}{s_\beta}$	$\frac{s_\alpha}{s_\beta}$	$\frac{c_\alpha}{c_\beta}$	$\frac{s_\alpha}{s_\beta}$	$\frac{1}{t_\beta}$	t_β	$-\frac{1}{t_\beta}$

Table I: The Yukawa coupling modifiers in four types of the 2HDM.

where six are free parameters from Eq. (4). The range of $\beta - \alpha$ is set to be $[-\pi/2, \pi/2]$, following the notation of the public codes such as 2HDMC [77], HIGGSIGNALS [78], and HIGGSBOUNDS [79], which results in $c_{\beta-\alpha} > 0$. Since one of our main results is from the RGE evolution of the quartic couplings, we present the quartic couplings [80]

$$\begin{aligned}
\lambda_1 &= \frac{1}{v^2 c_\beta^2} [c_\alpha^2 M_H^2 + s_\alpha^2 m_h^2 - t_\beta m_{12}^2], \\
\lambda_2 &= \frac{1}{v^2 s_\beta^2} \left[s_\alpha^2 M_H^2 + c_\alpha^2 m_h^2 - \frac{1}{t_\beta} m_{12}^2 \right], \\
\lambda_3 &= \frac{1}{v^2} \left[2M_{H^\pm}^2 + \frac{s_{2\alpha}}{s_{2\beta}} (M_H^2 - m_h^2) - \frac{m_{12}^2}{s_\beta c_\beta} \right], \\
\lambda_4 &= \frac{1}{v^2} \left[M_A^2 - 2M_{H^\pm}^2 + \frac{m_{12}^2}{s_\beta c_\beta} \right], \\
\lambda_5 &= \frac{1}{v^2} \left[\frac{m_{12}^2}{s_\beta c_\beta} - M_A^2 \right],
\end{aligned} \tag{6}$$

where $M^2 = m_{12}^2 / (s_\beta c_\beta)$.

According to the Z_2 parity of the fermion singlets, there are four different types in the 2HDM, type-I, type-II, type-X, and type-Y. According to the type, the Yukawa couplings to the SM fermions are different, but the gauge couplings remain the same. We parameterize the Yukawa Lagrangian as

$$\begin{aligned}
\mathcal{L}_{\text{Yuk}} &= - \sum_f \left(\frac{m_f}{v} \xi_f^h \bar{f} f h + \frac{m_f}{v} \xi_f^H \bar{f} f H - i \frac{m_f}{v} \xi_f^A \bar{f} \gamma_5 f A \right) \\
&\quad - \left\{ \frac{\sqrt{2} V_{ud}}{v} H^+ \bar{u} (m_u \xi_u^A P_L + m_d \xi_d^A P_R) d + \frac{\sqrt{2} m_\ell}{v} H^+ \xi_\ell^A \bar{\nu}_L \ell_R + \text{H.c.} \right\},
\end{aligned} \tag{7}$$

where $\xi_f^{h,H,A}$, the Yukawa coupling modifiers, are presented in Table I. Since we shall consider a total of eight cases, four types in the NS and IS, we shall use a simple notation of NS-I (IS-I) for type-I in the NS (IS), for instance.

Before scanning the whole parameter space, we study the implication of the oblique parameter T on the masses of new Higgs bosons in a simple setup, the normal scenario in the Higgs alignment limit. We consider two different Peskin-Takeuchi oblique parameter sets with $U = 0$,

before and after the new CDF m_W measurement, denoted by ‘‘PDG’’ and ‘‘CDF’’ respectively:

$$\text{PDG: } S = 0.05 \pm 0.08, \quad T = 0.09 \pm 0.07, \quad \rho_{ST} = 0.92, \quad (8)$$

$$\text{CDF: } S = 0.15 \pm 0.08, \quad T = 0.27 \pm 0.06, \quad \rho_{ST} = 0.93,$$

where ρ_{ST} is the correlation between S and T .

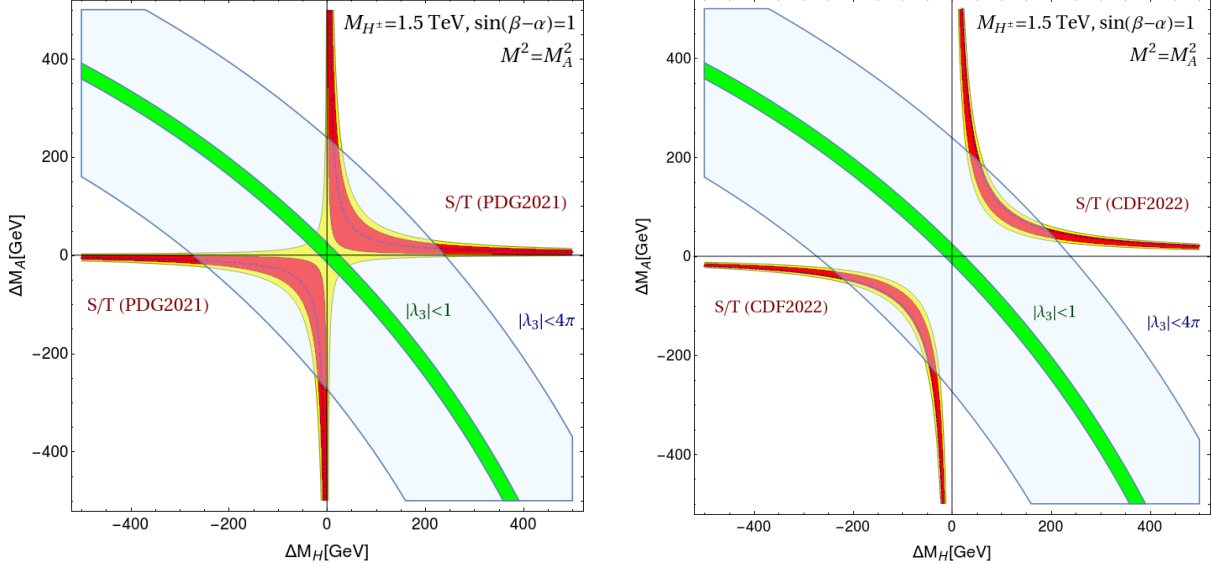


Figure 1: Allowed regions of $(\Delta M_H, \Delta M_A)$ by the oblique parameters of S and T (red at 1σ and yellow in 2σ), $|\lambda_3| < 4\pi$ (light blue), and $|\lambda_3| < 1$ (green), where $\Delta m \equiv m - M_{H^\pm}$. The left (right) panel shows the PDG (CDF) result. We set $M_{H^\pm} = 1.5$ TeV and $M^2 = M_A^2$ in the normal scenario with $s_{\beta-\alpha} = 1$.

As shall be shown, one of the most important results of the CDF-updated S/T is that there exist the upper bounds on the masses of new Higgs bosons even in the NS, which is not expected. This is due to the combined constraints from the theoretical stability, the new S/T , and $\Lambda_c > 1$ TeV. To understand why very heavy new Higgs bosons are excluded, we present the allowed regions of $(\Delta M_H, \Delta M_A)$ for $M_{H^\pm} = 1.5$ TeV by the oblique parameters S and T (red), $|\lambda_3| < 4\pi$ (light blue), and $|\lambda_3| < 1$ (green) in Fig. 1, where $\Delta m \equiv m - M_{H^\pm}$. The PDG result is in the left panel, and the CDF result is in the right panel. For illustration, we take a simple setup, the NS in the Higgs alignment limit. The condition of $M^2 = M_A^2$ is motivated to avoid excessively fast running of the quartic couplings in the RGE studies of the 2HDM [80].

While the PDG T parameter allows the total mass degeneracy of $M_{H^\pm} = M_A = M_H$ at 2σ level, the CDF-updated T prohibits it. Instead, the CDF result leaves two separate regions of the hyperbola-like shape. Despite the absence of the total mass degeneracy, the oblique T parameter from the CDF result still permits heavy masses of new Higgs bosons: when $M_H \approx M_{H^\pm}$ ($M_A \approx M_{H^\pm}$), very heavy M_A (M_H) is feasible. When applying the perturbativity of λ_3 (light blue), however, large mass gaps of ΔM_H and ΔM_A are forbidden. When narrowing

the range into $|\lambda_3| < 1$, there is no overlap with the allowed space by the CDF-updated T parameter. The $|\lambda_3|$ above one at the electroweak scale invokes its fast running under the RGE evolution, thus bringing the breakdown of the theory at the low energy scale by the RGE. Therefore, heavy Higgs bosons with masses above about 1 TeV cannot simultaneously satisfy the theoretical stability, the CDF-updated T parameter, and $\Lambda_c > 1$ TeV.

III. SCANNING STRATEGIES

We study the implication of the theoretical and experimental constraints through random scanning of the model parameters. The scanning ranges in the NS and IS are

$$\begin{aligned} \text{NS: } M_H &\in [130, 2000] \text{ GeV}, \quad M_A \in [15, 2000] \text{ GeV}, \\ s_{\beta-\alpha} &\in [0.8, 1.0], \quad m_{12}^2 \in [0, 1000^2] \text{ GeV}^2, \\ \text{IS: } m_h &\in [15, 120] \text{ GeV}, \quad M_A \in [15, 2000] \text{ GeV}, \\ c_{\beta-\alpha} &\in [0.8, 1.0], \quad m_{12}^2 \in [0, 1000^2] \text{ GeV}^2. \end{aligned} \quad (9)$$

The range of $s_{\beta-\alpha}$ is set comfortably, although the most updated results on the Higgs coupling modifiers are $\kappa_Z > 0.86$ and $\kappa_W > 0.94$ with $\kappa_{W,Z} \leq 1$ at 95% C.L. [81]. The parameters in Eq. (9) are independent of the type, but M_{H^\pm} and t_β are different because of the FCNC observables [71, 72]: M_{H^\pm} in type-II and type-Y is tightly constrained to be $M_{H^\pm} \gtrsim 580$ GeV; M_{H^\pm} in type-I and type-X can be as light as about 100 GeV. Therefore, we take the following ranges for M_{H^\pm} and t_β :

$$\begin{aligned} \text{type-I \& type-X: } M_{H^\pm} &\in [80, 2000] \text{ GeV}, \quad t_\beta \in [1, 50], \\ \text{type-II \& type-Y: } M_{H^\pm} &\in [580, 2000] \text{ GeV}, \quad t_\beta \in [0.5, 50]. \end{aligned} \quad (10)$$

With the prepared random parameter points, we cumulatively impose the following steps for the theoretical and experimental constraints:

Step-(i) Theory+FCNC: We require a parameter point to satisfy the theoretical stabilities and the FCNC results, by using the public code 2HDMC-v1.8.0 [77].

1. Higgs potential being bounded from below [82];
2. Perturbative unitarity of the amplitudes of scalar-scalar, scalar-vector, and vector-vector scatterings at high energies [83, 84];
3. Perturbativity of the quartic couplings [73, 85];
4. Vacuum stability [86].
5. FCNC observables: In type-I and type-X, the viable space of (M_{H^\pm}, t_β) is determined practically by $b \rightarrow s\gamma$ [71, 72]. In type-II and type-Y, on the other hand, ΔM_{B_s} [87] is more important in constraining the region with $M_{H^\pm} \gtrsim 650$ GeV.

Step-(ii) EWPD: We calculate the Peskin-Takeuchi oblique parameters in the 2HDM [88–90], and compare them with the oblique parameters fitted to the EWPD before and after the CDF m_W measurement. Since we perform two parameter (S and T) fitting under the assumption of $U = 0$, we require $\chi^2 < 5.9$.

Step-(iii) RGEs for $\Lambda_c > 1$ TeV: We require that the model should be valid at least up to 1 TeV. Using the RGE’s [73, 80, 91–93], we run the dimensionless parameters in the 2HDM, including the gauge couplings, the quartic couplings in the scalar potential, and the Yukawa couplings of the top quark, bottom quark, and tau lepton. The initial conditions of the gauge couplings and the Yukawa couplings are set at the top quark mass scale $m_t = 173.34$ GeV [94]. As increasing the energy scale, we check the unitarity and stability conditions. If any condition is broken at the energy scale below 1 TeV, we exclude the parameter point. In other words, the cutoff scale Λ_c of the model should be above 1 TeV. We use the public code 2HDME-v1.2 [94] at one-loop level.

Step-(iv) Collider: The collider constraints consist of two categories, the Higgs precision data and the direct search bounds at the LEP, Tevatron, and LHC. To check the consistency with the Higgs precision, we use HIGGSIGNALS-v2.6.2 [78], which yields the χ^2 output for 111 Higgs observables [95–102]. Since there are six model parameters, the number of degrees of freedom is 105. We demand that the p -value be larger than 0.05. For the consistency with the direct searches at high energy collider, we use the public code, HIGGSBOUNDS-v5.10.2 [79]. For each process at the LEP, Tevatron, and LHC, we calculate the cross section in the model, and compare it with the upper bound on the cross section at the 95% C.L. When the model prediction is above the observed upper bound, we exclude the parameter point.

We perform the random scan over the entire six-dimensional parameter space. For each type in the NS and IS (eight cases), we obtained 10^6 parameter points that satisfy Step-(i), which is to be the reference when computing the survival probabilities. Before proceeding to the subsequent steps, we investigate the implications of Step-(i) on the masses of new Higgs bosons. In Fig. 2, we present the parameter points in (M_H, M_A) that pass Step-(i), where the color codes denote M_{H^\pm} . The results in the NS (IS) are in the upper (lower) panels and those at type-I/X (type-II/Y) are in the left (right) panels.

The theoretical stabilities and the FCNC observables significantly restrict the masses of new Higgs bosons. In the NS, the low mass regions with $M_A, M_H, M_{H^\pm} \lesssim 750$ GeV are uniformly permitted, without a correlation among the masses. For the high mass above 750 GeV, however, Step-(i) demands a considerable correlation among the masses, preferring small mass gaps and thus the mass degeneracy. The higher the mass scales are, the smaller the mass gaps will be. In the IS, Step-(i) already puts the upper bounds on M_A and M_{H^\pm} , below about 750 GeV.

Now we cumulatively impose the constraints of Step-(ii), Step-(iii), and Step-(iv). In Table

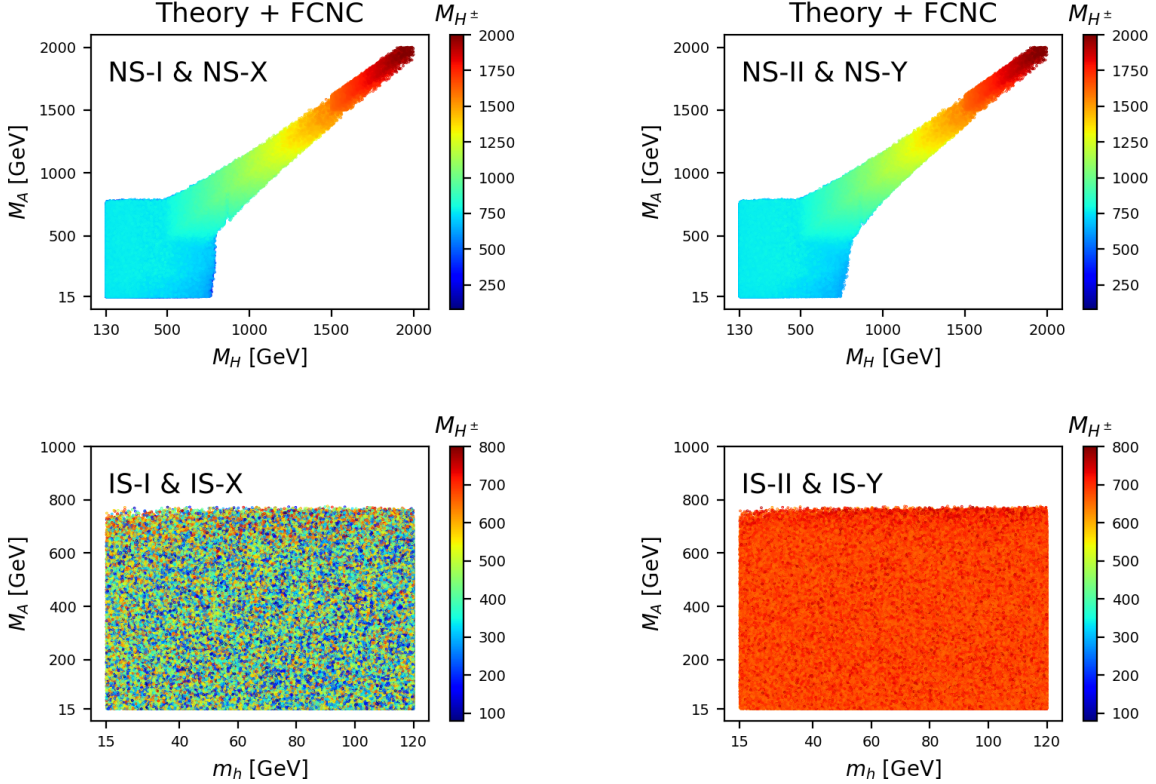


Figure 2: Allowed regions of (M_H, M_A) in the NS (upper panels) and (m_h, M_A) in the IS (lower panels) by the theoretical stabilities and the $b \rightarrow s\gamma$ constraint. The results in type-I and type-X are in the left panels, while those in type-II and type-Y are in the right panels. The color codes indicate M_{H^\pm} .

II, we present the survival probabilities of the random scanning in Eqs. (9) and (10)¹ at each step in the NS and IS for all the four types, with respect to the parameter points that pass Step-(i). One of the most important features is that the combination of all the theoretical and experimental constraints restricts the model more severely for the CDF result than for the PDG: see two figures in the right panels.

Let us compare the overall differences between the NS and IS. In the NS, all the types survive the final Step-(iv), even though the survival probabilities are very small, of the order of 0.1% (0.01%) for the PDG (CDF) result. We find that type-I has the largest survival probabilities while type-II and type-Y have the smallest probabilities. In the IS, type-II and type-Y are totally excluded.² The decisive factor is the combination of $M_{H^\pm} > 580$ GeV from $b \rightarrow s\gamma$ and the requirement of $\Lambda_c > 1$ TeV. The constraint from $b \rightarrow s\gamma$ demands heavy Higgs masses, which brings out too fast running of the quartic couplings. Type-I and type-X are still allowed

¹ The survival probabilities depend on the scanning ranges. For smaller ranges, the probabilities increase.

² To confirm this finding, we increased the number of points in random scanning. But no parameter point survived for type-II and type-Y in the IS.

		EWPD	$\Lambda_c > 1$ TeV	Collider	EWPD	$\Lambda_c > 1$ TeV	Collider
		Normal scenario			Inverted scenario		
type-I	PDG	12.98%	5.13%	0.60%	7.20%	5.08%	0.85%
	CDF	4.42%	1.31%	0.14%	1.30%	0.72%	0.19%
type-II	PDG	10.76%	0.43%	0.20%	2.14%	0	0
	CDF	3.36%	0.03%	0.01%	0.69%	0	0
type-X	PDG	12.98%	5.13%	0.18%	7.20%	5.08%	0.03%
	CDF	4.42%	1.31%	0.03%	1.30%	0.72%	0.01%
type-Y	PDG	10.76%	0.43%	0.20%	2.14%	0	0
	CDF	3.36%	0.03%	0.01%	0.69%	0	0

Table II: Survival probabilities at each step in the NS and IS for all the four types, with respect to the parameter points that pass Step (i). For the EWPD, we adopt two different schemes of the oblique parameters, before and after the CDF-updated m_W measurement, denoted by “PDG” and “CDF”.

in the IS.

Now we study the differences between the PDG and CDF results. As shown in Table II, the survival probabilities are very different, which are much small for the CDF result in all the eight cases. The probability gap between the PDG and CDF results widens sharply at Step-(ii). It is coming from the tension that the EWPD prefer sizable ΔM_A and $\Delta M_{h,H}$ but $\Lambda_c > 1$ TeV favors the mass degeneracy [80]. Step-(iv) including the Higgs precision data and the direct search bounds also reduces the parameter space substantially, in both cases with the PDG and CDF results.

To demonstrate the origin of the differences between the PDG and CDF in more detail, we present the parameter points of (M_H, M_A) that survive each step. In Fig. 3, we consider type-I in the NS. At Step-(ii), the PDG and CDF cases yield similar shapes also in the heavy mass regions. But the size is different: the CDF result generates a slimmer area with substantial mass gaps, while the PDG case allows a broader area, including $M_H = M_A = M_{H^\pm}$. Existence or absence of the total mass degeneracy decides whether to save the heavy mass region when imposing $\Lambda_c > 1$ TeV. Therefore, the combination of the theoretical constraint with $\Lambda_c > 1$ TeV puts the upper bounds on the masses of new Higgs bosons in the CDF case. Applying the constraints from the Higgs precision data and the direct collider searches at Step-(iv) reduces the viable parameter points, but the upper bounds on new Higgs bosons remain intact.

Figure 4 presents the same results for type-II, where $M_{H^\pm} > 580$ GeV due to the constraints from FCNC. As in type-I, the EWPD before and after the CDF m_W measurement yield similar shapes in M_H vs M_A with color code of M_{H^\pm} . Sizable mass gaps are also required in the CDF case. A dramatic difference occurs when we further impose $\Lambda_c > 1$ TeV, which puts the upper bounds on the masses of new Higgs bosons and the lower bounds on M_H and M_A . At the final Step-(iv), a large portion of the parameter points is further excluded, but the mass bounds of

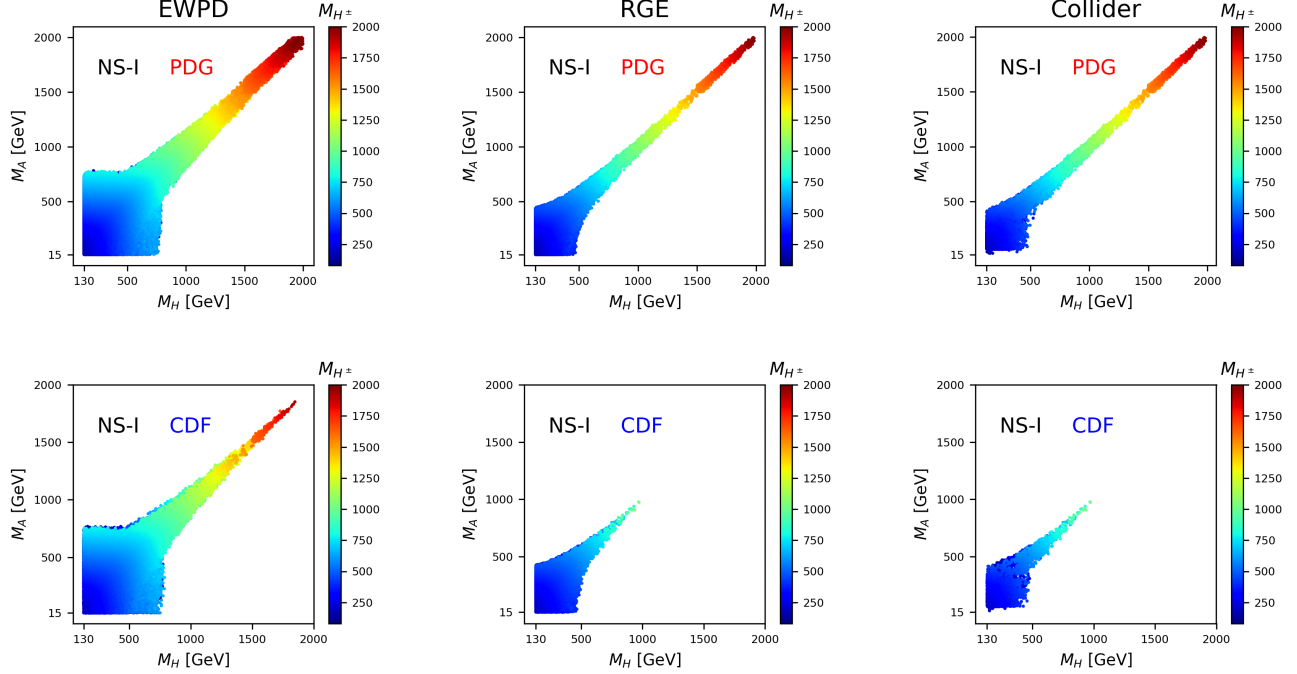


Figure 3: In type-I of the normal scenario, the allowed parameter space of (M_H, M_A) after Step-(ii) (EWPD), Step-(iii) (Step(ii)+RGE), and Step-(iv) (Step(iii)+Higgs precision+Direct searches), with the color code indicating M_{H^\pm} . The upper panels are for PDG while the lower panels for CDF.

new Higgs bosons remain almost intact.

In summary, we present the allowed mass ranges in the NS:

$$\text{NS-I: } M_{H^\pm} \in [87, 1060] \text{ GeV}, \quad M_H \in [130, 971] \text{ GeV}, \quad M_A \in [28, 977] \text{ GeV}; \quad (11)$$

$$\text{NS-II: } M_{H^\pm} \in [600, 1139] \text{ GeV}, \quad M_H \in [427, 1127] \text{ GeV}, \quad M_A \in [470, 1125] \text{ GeV};$$

$$\text{NS-X: } M_{H^\pm} \in [110, 1060] \text{ GeV}, \quad M_H \in [130, 971] \text{ GeV}, \quad M_A \in [48, 977] \text{ GeV};$$

$$\text{NS-Y: } M_{H^\pm} \in [600, 1139] \text{ GeV}, \quad M_H \in [427, 1127] \text{ GeV}, \quad M_A \in [470, 1125] \text{ GeV};$$

and in the IS:

$$\text{IS-I: } M_{H^\pm} \in [166, 436] \text{ GeV}, \quad m_h \in [47, 120] \text{ GeV}, \quad M_A \in [55, 411] \text{ GeV}; \quad (12)$$

$$\text{IS-X: } M_{H^\pm} \in [170, 435] \text{ GeV}, \quad m_h \in [64, 120] \text{ GeV}, \quad M_A \in [28, 409] \text{ GeV}.$$

It is noteworthy that a light charged Higgs boson with mass around 100 GeV is feasible in the NS-I [103].

IV. CHARACTERISTIC FEATURES OF THE NORMAL SCENARIO

In this section, we study the characteristics of the finally allowed parameters after the CDF m_W measurement, focusing on the NS. Since the results of type-I (type-II) are similar to those

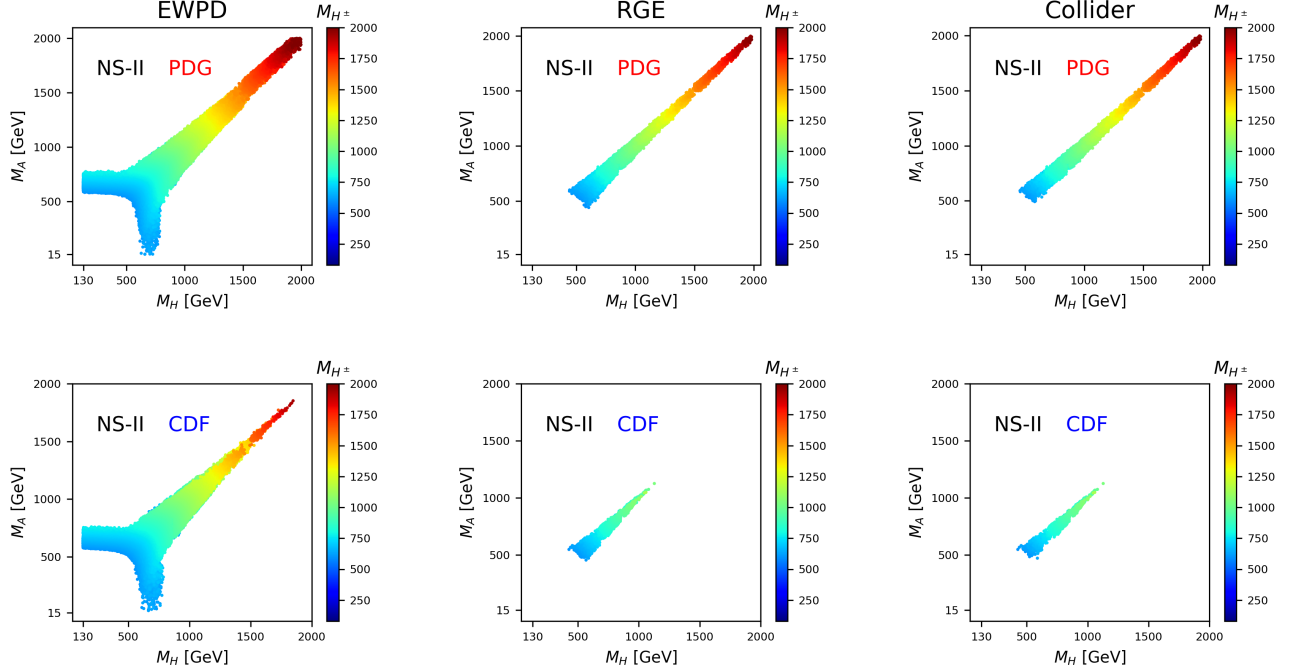


Figure 4: In type-II of the normal scenario, the allowed parameter space of (M_H, M_A) after Step-(ii), Step-(iii), and Step-(iv), with the color code indicating M_{H^\pm} . The upper panels are for PDG while the lower panels for CDF.

of type-X (type-Y), we show the results of type-I and type-X (type-II and type-Y) together. We shall sequentially present the parameter points according to the steps when needed. For a more detailed understanding, we separate Step-(iv) into two, one for the Higgs precision data and the other for the direct search bounds at the LHC. In summary, the order of the *cumulative* steps is as follows: (1) Theory+FCNC; (2) EWPD for the oblique parameters of S and T ; (3) RGE study for $\Lambda_c > 1$ TeV; (4) Higgs precision data through HIGGSIGNALS; (5) Direct search bounds through HIGGSBOUNDS.

A. type-I and type-X

First, we take a closer look at the allowed masses at the final Step-(iv). In Fig 5, we present M_H vs M_A with color code of M_{H^\pm} in type-I (left panel) and type-X (right panel). In the heavy mass region with $M_H, M_A \gtrsim 700$ GeV, a strong correlation exists among the masses of new Higgs bosons. We found that both ΔM_H and ΔM_A are clustered around $\Delta M_{H,A} \simeq -100$ GeV and $\Delta M_{H,A} \simeq 100$ GeV: more points are in the negative $\Delta M_{H,A}$ region. For $M_H, M_A \lesssim 700$ GeV, there is little correlation among masses. Compared with the results at the Step-(i) as shown in Fig. 2, however, similar mass scales are weakly favored in the end.

Now we move on to $|s_{\beta-\alpha}|$ vs t_β . Figure 6 presents their correlation in type-I (upper panels) and type-X (lower panels), with color code indicating M_{H^\pm} . We compare the result in the PDG

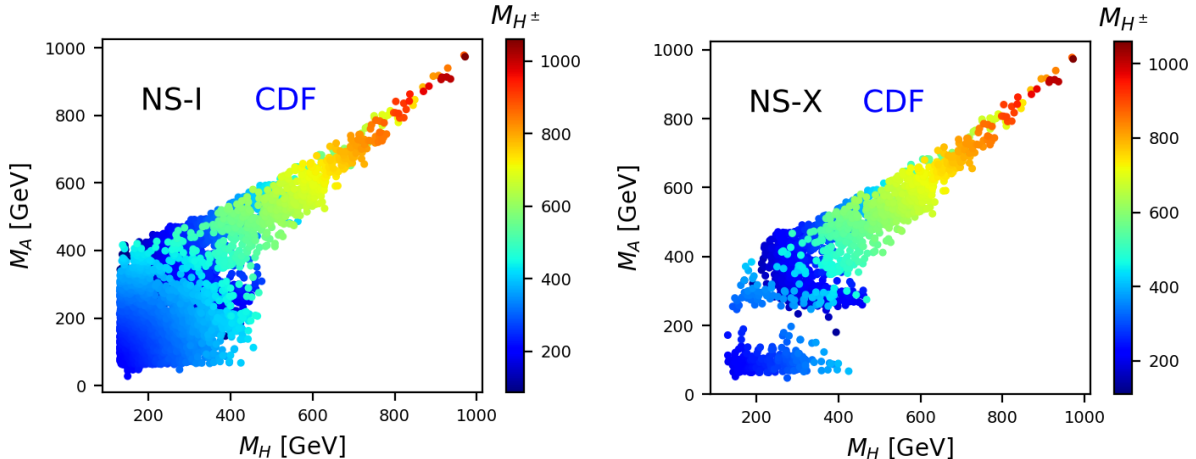


Figure 5: M_H vs M_A with color code of M_{H^\pm} in type-I (left panel) and type-X (right panel) in the CDF case. We adopt the normal scenario.

case (left panels) with that in the CDF case (right panels). For $|s_{\beta-\alpha}|$, the Higgs precision data play a vital role in limiting it as $|s_{\beta-\alpha}| \gtrsim 0.88$ in type-I and $|s_{\beta-\alpha}| \gtrsim 0.90$ in type-X, which are almost the same both before and after the CDF m_W anomaly. Interestingly, the upper bound on t_β is considerably small in the CDF case. In type-I, most of the surviving points have $t_\beta \lesssim 45$ in the CDF case, which was $t_\beta \lesssim 50$ in the PDG case. The larger t_β is, the more fermiphobic the new Higgs bosons are in type-I because all the fermion Yukawa couplings to H , A , and H^\pm are inversely proportional to t_β . So, the reduced upper bounds on t_β increase the LHC discovery potential of new Higgs bosons through fermionic production and decay channels. In type-X, the points with $t_\beta \gtrsim 30$ are all excluded in the CDF case: in the PDG case, however, $t_\beta \gtrsim 35$ is prohibited. We also observe that the heavy charged Higgs boson with mass above ~ 700 GeV demands the almost exact Higgs alignment limit.

An intriguing difference between type-I and type-X appears in the positive and negative $s_{\beta-\alpha}$ regions,³ when imposing the Higgs precision data. Figure 7 shows $s_{\beta-\alpha}$ vs t_β in type-I (left panel) and type-X (right panel). We separately display the parameter points satisfying $\Lambda_c > 1$ TeV (gray) and the points consistent with the Higgs precision data (yellow): yellow points are on top of gray points. At Step (iii), both the positive and negative $s_{\beta-\alpha}$ have almost symmetric regions. Type-I almost keeps the symmetric shape when imposing the Higgs precision data, but type-X does not. The part with negative $s_{\beta-\alpha}$ is excluded chiefly, except for the Higgs alignment limit.

Such a difference between type-I and type-X comes from the tau Yukawa coupling to the

³ In the scheme of $s_{\beta-\alpha} > 0$, as usually adopted in many phenomenology studies, positive and negative $s_{\beta-\alpha}$ correspond to the positive and negative $c_{\beta-\alpha}$, respectively.

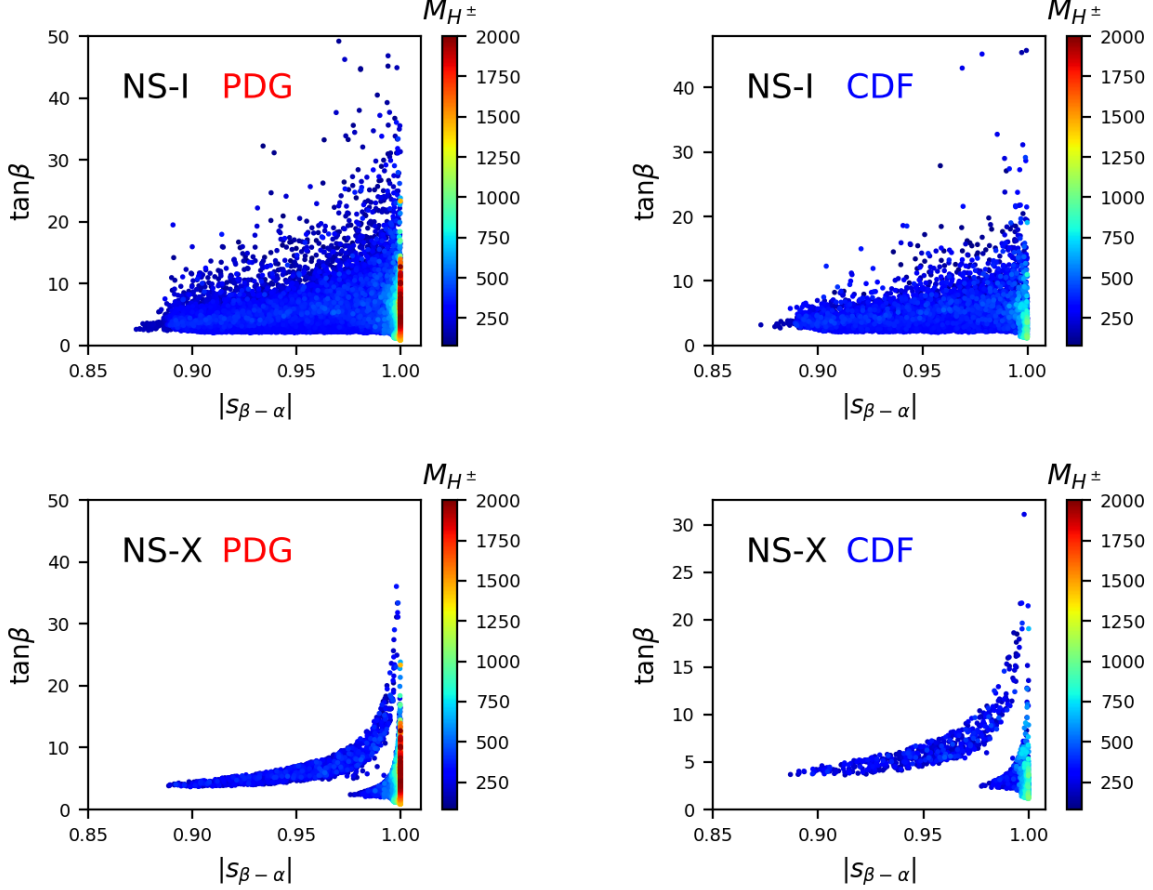


Figure 6: Allowed regions of $(|s_{\beta-\alpha}|, t_\beta)$ in type-I (upper panels) and type-X (lower panels), with color code indicating M_{H^\pm} for the normal scenario. We compare the results before (left panels) and after (right panels) the CDF m_W measurement.

Higgs boson h in Table I:

$$\text{type-I: } \xi_\tau^h = \frac{c_\alpha}{s_\beta} = s_{\beta-\alpha} + \frac{c_{\beta-\alpha}}{t_\beta}, \quad (13)$$

$$\text{type-X: } \xi_\tau^h = -\frac{s_\alpha}{c_\beta} = s_{\beta-\alpha} - t_\beta c_{\beta-\alpha}. \quad (14)$$

In type-I, the $c_{\beta-\alpha}$ term is suppressed by large t_β so the negative $s_{\beta-\alpha}$ does not change $|\xi_\tau^h|$ much. In type-X, however, the $c_{\beta-\alpha}$ term is proportional to t_β and thus non-negligible. Negative $s_{\beta-\alpha}$ excessively increases $|\xi_\tau^h|$ so that the branching ratio of $h \rightarrow \tau^+\tau^-$ exceeds the experimental bound. Most of the negative $s_{\beta-\alpha}$ region is excluded, except for almost the exact alignment limit. The appearance of the “arm” region in the positive $s_{\beta-\alpha}$ case of type-X can also be explained by Eq. (14). When $t_\beta \simeq 2/c_{\beta-\alpha}$, $\xi_\tau^h (\simeq s_{\beta-\alpha} - 2)$ approaches -1 when $s_{\beta-\alpha} \simeq 1$. We have the wrong-sign limit for the tau lepton. It is to be compared with the wrong-sign limit in type-II where both the bottom quark and tau lepton have the Yukawa couplings with the wrong sign.

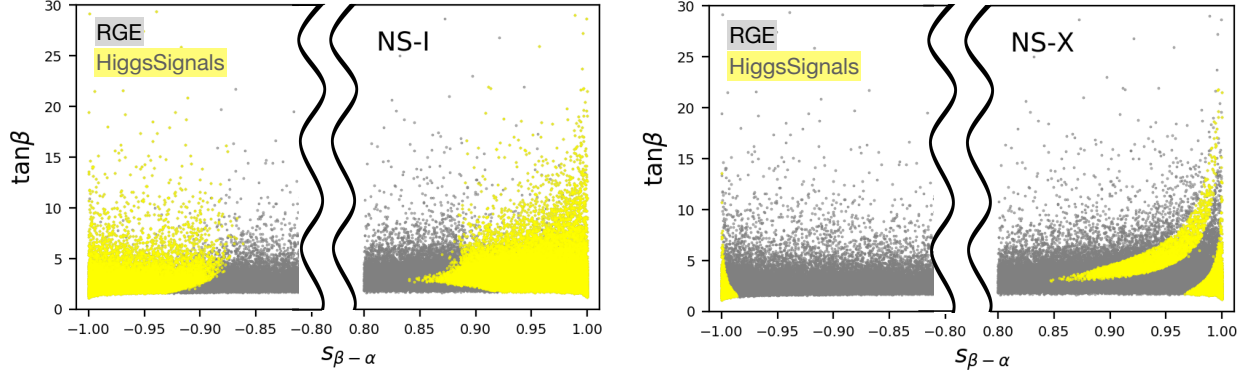


Figure 7: Allowed parameter points of $(s_{\beta-\alpha}, t_\beta)$ in type-I (left panel) and type-X (right panel) of the normal scenario that pass the RGE (gray) and the Higgs precision data (yellow).

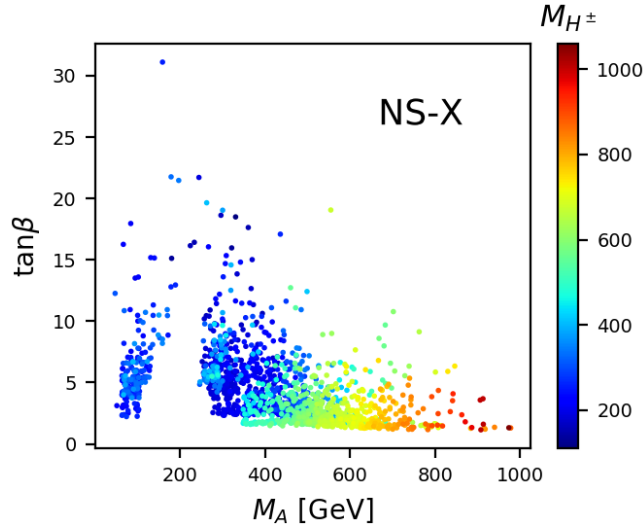


Figure 8: In type-X of the normal scenario, the allowed parameter points of (M_A, t_β) at the final Step-(iv). The color code denotes M_{H^\pm} .

Finally, we find that M_A in type-X is strongly constrained by the direct search bounds at the LHC. In Fig. 8, we present M_A vs t_β , with the color code indicating M_{H^\pm} . Particularly for $t_\beta \lesssim 10$, the intermediate M_A around 200 GeV is excluded. A major reason is that the masses of both H and A are similar to M_{H^\pm} : see Fig. 3. As H and A are within the LHC reach, several direct search processes exclude the $M_A \sim 200$ GeV region. The first three important processes, in order of importance, are $t \rightarrow H^\pm b \rightarrow \tau \nu b$ [104], $pp \rightarrow H \rightarrow \tau^+ \tau^-$ [105, 106], and $gg \rightarrow A \rightarrow Zh \rightarrow \ell \ell b \bar{b}$ [107].

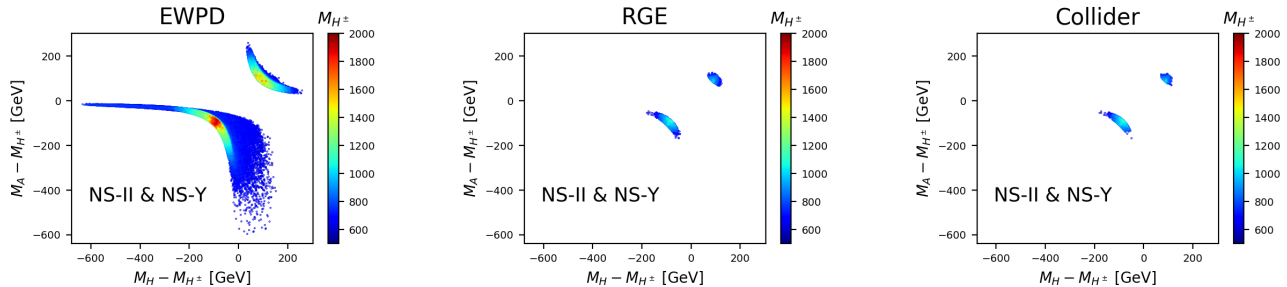


Figure 9: In type-II and type-Y of the normal scenario, the allowed parameter points of $(\Delta M_H, \Delta M_A)$ at the Step-(ii) in the left panel, at the Step-(iii) in the middle panel, and at the Step-(iv) in the right panel, where $\Delta m \equiv m - M_{H^\pm}$. The color code denotes M_{H^\pm} .

B. type-II and type-Y

At every step, the viable parameter points in type-II are very similar (almost indistinguishable from the eyes) to those in type-Y. So, the results in this subsection apply to both type-II and type-Y.

In type-II and type-Y, the biggest impact comes from the condition of $\Lambda_c > 1$ TeV. Figure 9 shows the allowed parameter points of $(\Delta M_H, \Delta M_A)$ at the Step-(ii) in the left panel, at the Step-(iii) in the middle panel and at the Step-(iv) in the right panel. The EYPD data after the CDF m_W measurement allow the hyperbola-shape with a sufficiently large mass gaps of ΔM_H and ΔM_A : see Fig. 1.⁴ Imposing $\Lambda_c > 1$ TeV drastically curtails the parameter space of $(\Delta M_H, \Delta M_A)$, excluding the mass gaps above around 200 GeV. In addition, the positive $\Delta M_{H,A}$ case is more severely restricted by $\Lambda_c > 1$ TeV, leaving a much smaller allowed region. It is because the heavy Higgs bosons invoke fast running of the quartic couplings, failing the unitarity and vacuum stability at the energy scale below 1 TeV. The constraints from the collider data do not change ΔM_H vs ΔM_A much. these.

Finally, a brief discussion on the constraint from $b \rightarrow s\gamma$ is in order here. We took a conservative bound on the charged Higgs boson mass as $M_{H^\pm} \gtrsim 580$ GeV for consistency with the FCNC observables. But the bound considerably increases to about 800 GeV if we adopt the calculation of the NNLO QCD corrections to $\mathcal{B}(\bar{B} \rightarrow X_s \gamma)$ in the SM without the interpolation in the charm quark mass [108]. There still exist certain parameter points like $800 \text{ GeV} \lesssim M_{H^\pm} \lesssim 1100 \text{ GeV}$. But the survival rate is very small: only 34 parameter points out of 10^6 points, which satisfy Step-(i), pass the final Step-(iv) for $M_{H^\pm} > 800$ GeV. Obviously, the limited M_{H^\pm} restricts other model parameters. Figure 10 shows the finally viable parameter points in (M_H, M_A) (left panel) and in $(|s_{\beta-\alpha}|, t_\beta)$ (right panel), with color code of M_{H^\pm} . To thoroughly investigate the status of type-II and type-Y with $M_{H^\pm} > 800$ GeV, we additionally

⁴ Negative $\Delta M_{H,A}$ region is different from Fig. 1. The difference is attributed to the assumption of the Higgs alignment limit in Fig. 1. Our main results do not depend on any prerequisites for the model parameters.

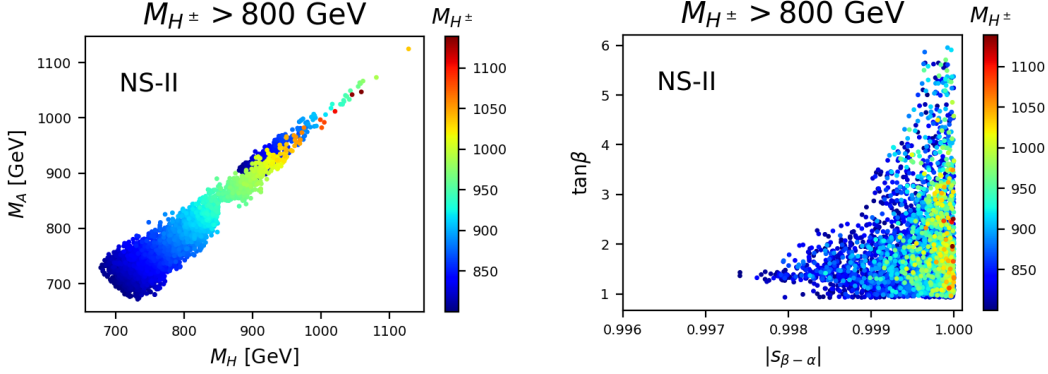


Figure 10: For type-II and type-Y in the normal scenario, the allowed parameter points of $(\Delta M_H, \Delta M_A)$ in the left panel and $(|s_{\beta-\alpha}|, t_\beta)$ in the right panel at the final Step-(iv) with $M_{H^\pm} > 800$ GeV from the $b \rightarrow s\gamma$ constraint. The color code denotes M_{H^\pm} .

generated parameter points focusing on this particular region. Both M_H and M_A (left panel) are accordingly constrained to be $[670, 1000]$ GeV, slightly relaxed than M_{H^\pm} . The restriction to $|s_{\beta-\alpha}|$ and t_β (right panel) are stronger. The Higgs alignment limit is almost exact, within about 0.2%, and t_β is in $[1, 5]$.

V. CHARACTERISTIC FEATURES OF THE INVERTED SCENARIO

As shown in Table II, type-II and type-Y in the IS are excluded by the condition of $\Lambda_c > 1$ TeV. Therefore, we focus on type-I and type-X in this section.

The first remarkable feature of the IS is the considerably different survival probabilities between type-I and type-X. In Fig. 11, we show the parameter points of (m_h, M_A) at the steps of $\Lambda_c > 1$ TeV (left panels), the Higgs precision data (middle panels), and the direct search bounds (right panels) for type-I (upper panels) and type-X (lower panels) in the IS. At the RGE step, type-I and type-X yield almost the same results. A significant difference arises when imposing the Higgs precision data: the allowed points in type-X are more sparsely dense than those in type-I. The direct search bounds further widen the difference. In type-X, only about 0.03% of the parameter space survives, which is to be compared with about 0.77% in type-I. The leptophilic nature of type-X, being more severe for large t_β , plays an essential role in this considerable curtailment. A significant result at the final step is that in type-I, there exist some parameter points with m_h below $m_{125}/2$, while in type-X, all the parameter points with $m_h < 62.5$ GeV are excluded.

The second noteworthy feature is the strong correlation of M_A and m_h to M_{H^\pm} . Figure 12 shows the allowed parameter points of $(\Delta m_h, \Delta M_A)$ at the final step for type-I in the inverted scenario: the results in type-X are very similar, with sparse density. First of all, only the negative Δm_h and negative ΔM_A are allowed. As we have a relatively light mass spectrum for all the new Higgs bosons, the LHC is expected to have discovery potential. Another unanticipated

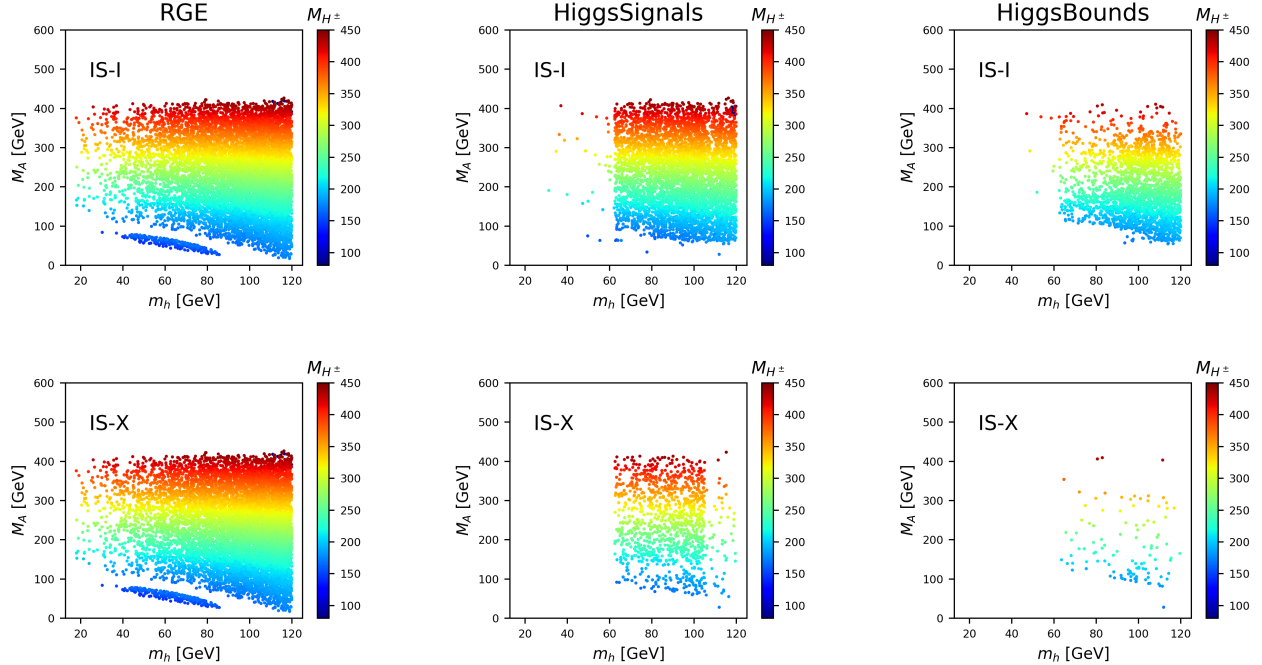


Figure 11: Allowed parameter points of (m_h, M_A) after imposing $\Lambda_c > 1$ TeV (left panels), the Higgs precision data (middle panels), and the direct search bounds (right panels) for type-I (upper panel) and type-X (lower panel) in the inverted scenario. The color code denotes M_{H^\pm} .

aspect is the approximate mass degeneracy of $M_{H^\pm} \simeq M_A$ for heavy M_{H^\pm} . For $M_{H^\pm} \gtrsim 350$ GeV, $|\Delta M_A| < 40$ GeV. We expect that this region is quite elusive at the LHC, especially for large t_β : the production rates of A and H^\pm through gluon fusion are suppressed by large t_β ; the decay of $H^\pm \rightarrow AW^{\pm*} \rightarrow Af\bar{f}'$ accompanying soft jets or leptons is also challenging to probe.

Finally, we present $|s_{\beta-\alpha}|$ vs t_β in Fig. 13 for type-I (left panel) and type-X (right panel) of the IS. The difference between type-I and type-X is considerable. In type-I, the deviation from the Higgs alignment limit is sizable. The value of $|s_{\beta-\alpha}|$ can be as large as about 0.48. In addition, large t_β around 50 is also permitted. In type-X, however, both $|s_{\beta-\alpha}|$ and t_β are more severely limited, like $|s_{\beta-\alpha}| \lesssim 0.2$ and $t_\beta \lesssim 30$. Only a small deviation from the Higgs alignment limit is permitted. Moreover, the very large t_β region in this leptophilic model is strongly constrained by the direct searches at the LHC, as in the NS.

VI. CONCLUSIONS

The recent m_W^{CDF} measurement by the CDF Collaboration has a significant impact on searching for physics beyond the standard model. In terms of the Peskin-Takeuchi parameters of S and T , the central values shift to larger values: $S = 0.15 \pm 0.08$, $T = 0.27 \pm 0.06$ with $U = 0$, which has profound consequences in searching for physics beyond the SM. We have illustrated in the framework of two-Higgs-doublet Models, including type-I, type-II, type-X, and type-

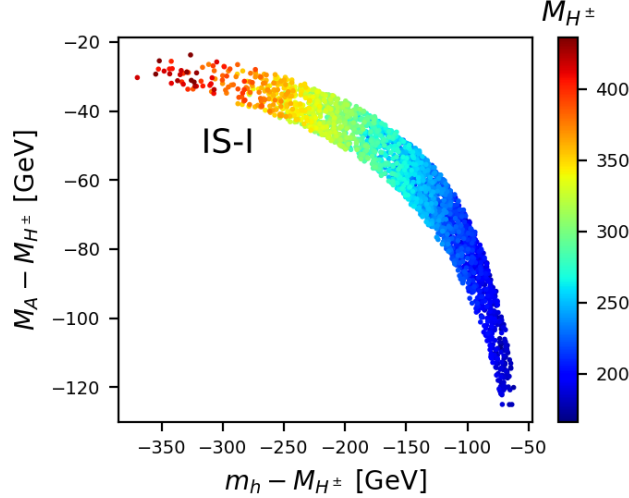


Figure 12: Allowed parameter points of $(\Delta m_h, \Delta M_A)$ at the final step for type-I in the inverted scenario, with color code of M_{H^\pm} .

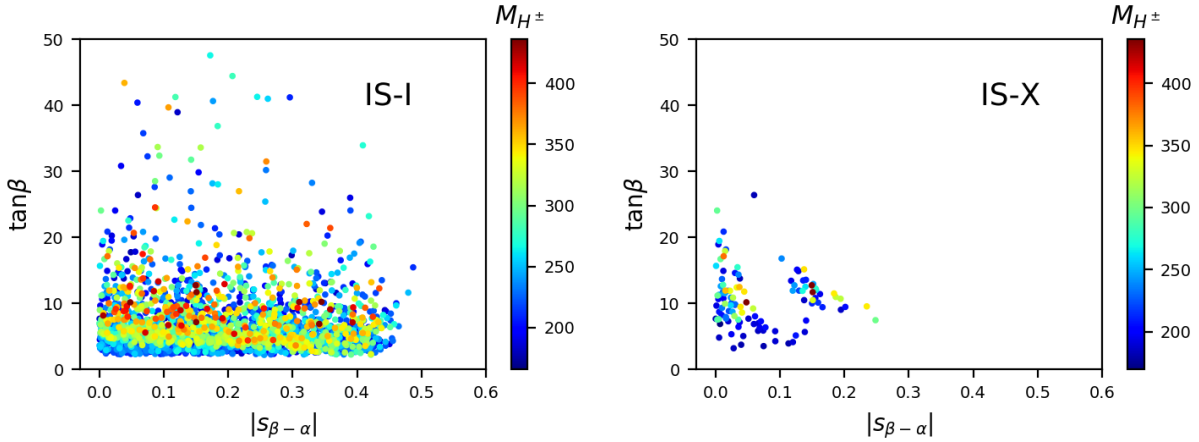


Figure 13: Allowed parameter points of $(|s_{\beta-\alpha}|, t_\beta)$ at the final step for type-I (left panel) and type-X (right panel) in the inverted scenario, with color code of M_{H^\pm} .

Y, the effects on the still-valid parameter space due to the new m_W^{CDF} together with other constraints, which include theoretical requirements (potential bounded from below, unitarity, perturbativity, vacuum stability), flavor-changing neutral currents in B physics, maintaining the perturbativity of the model until the cutoff scale $\Lambda_c = 1$ TeV, Higgs precision data, and direct collider search limits from the LEP, Tevatron, and LHC.

The most unprecedented consequence is the emergence of upper bounds on the masses of the heavy Higgs boson $M_{H,A,H^\pm} \lesssim 1000 - 1100$ GeV in the normal scenario and $M_{H^\pm,A} \lesssim 410 - 440$ GeV in the inverted scenario. Such interesting findings imply that the upcoming LHC run can readily close out the still-available parameter space.

Before closing, a few more findings from our study are offered as follows:

1. The updated fit on the oblique parameters of S and T indicates that the new m_W measurement requires larger mass splittings among the isospin components in multiplet models.
2. In subsequent steps of imposing constraints on the parameters, we found that the survival probabilities for the case of using the new m_W^{CDF} are much smaller than the case of using the PDG value, thus implying more restriction on physics beyond the SM (not only for 2HDM). This behavior has been demonstrated in all four types and two scenarios of 2HDM.
3. The $\tan\beta$ is bounded from above more severely when the new m_W^{CDF} value is used in the normal scenario. Roughly, $\tan\beta \lesssim 45, 6, 30, 10$ for type-I, II, X, and Y, respectively. On the other hand, $\tan\beta$ is not bounded in type I and $\tan\beta \lesssim 30$ for type X in the inverted scenario. There is no parameter space surviving all the requirements in type-II and type-Y of the inverted scenario.
4. If we raise the cutoff scale Λ_c beyond 1 TeV, the restriction on the parameter space would become more severe.

Acknowledgments

We would like to thank Dr. Jing-Hwan Cho of *National Institute for Mathematical Sciences* in Korea for helping the numerical computation. K.C. was supported by MoST with grant numbers MOST-110-2112-M-017-MY3. The work of JK, SL, and JS is supported by the National Research Foundation of Korea, Grant No. NRF-2022R1A2C1007583.

-
- [1] CDF collaboration, T. Aaltonen et al., *High-precision measurement of the W boson mass with the CDF II detector*, *Science* **376** (2022) 170–176.
 - [2] PARTICLE DATA GROUP collaboration, P. A. Zyla et al., *Review of Particle Physics*, *PTEP* **2020** (2020) 083C01.
 - [3] ALEPH, DELPHI, L3, OPAL, LEP ELECTROWEAK collaboration, S. Schael et al., *Electroweak Measurements in Electron-Positron Collisions at W -Boson-Pair Energies at LEP*, *Phys. Rept.* **532** (2013) 119–244, [[1302.3415](#)].
 - [4] LHCb collaboration, R. Aaij et al., *Measurement of the W boson mass*, *JHEP* **01** (2022) 036, [[2109.01113](#)].
 - [5] ATLAS collaboration, M. Aaboud et al., *Measurement of the W -boson mass in pp collisions at $\sqrt{s} = 7$ TeV with the ATLAS detector*, *Eur. Phys. J. C* **78** (2018) 110, [[1701.07240](#)].
 - [6] D0 collaboration, V. M. Abazov et al., *Measurement of the W Boson Mass with the D0 Detector*, *Phys. Rev. Lett.* **108** (2012) 151804, [[1203.0293](#)].

- [7] J. Haller, A. Hoecker, R. Kogler, K. Mönig, T. Peiffer and J. Stelzer, *Update of the global electroweak fit and constraints on two-Higgs-doublet models*, *Eur. Phys. J. C* **78** (2018) 675, [[1803.01853](#)].
- [8] J. de Blas, M. Ciuchini, E. Franco, A. Goncalves, S. Mishima, M. Pierini et al., *Global analysis of electroweak data in the Standard Model*, [2112.07274](#).
- [9] C.-T. Lu, L. Wu, Y. Wu and B. Zhu, *Electroweak Precision Fit and New Physics in light of W Boson Mass*, [2204.03796](#).
- [10] A. Strumia, *Interpreting electroweak precision data including the W-mass CDF anomaly*, [2204.04191](#).
- [11] J. de Blas, M. Pierini, L. Reina and L. Silvestrini, *Impact of the recent measurements of the top-quark and W-boson masses on electroweak precision fits*, [2204.04204](#).
- [12] J. Fan, L. Li, T. Liu and K.-F. Lyu, *W-Boson Mass, Electroweak Precision Tests and SMEFT*, [2204.04805](#).
- [13] A. Paul and M. Valli, *Violation of custodial symmetry from W-boson mass measurements*, [2204.05267](#).
- [14] J. Gu, Z. Liu, T. Ma and J. Shu, *Speculations on the W-Mass Measurement at CDF*, [2204.05296](#).
- [15] P. Asadi, C. Cesarotti, K. Fraser, S. Homiller and A. Parikh, *Oblique Lessons from the W Mass Measurement at CDF II*, [2204.05283](#).
- [16] M. Endo and S. Mishima, *New physics interpretation of W-boson mass anomaly*, [2204.05965](#).
- [17] R. Balkin, E. Madge, T. Menzo, G. Perez, Y. Soreq and J. Zupan, *On the implications of positive W mass shift*, [2204.05992](#).
- [18] L. M. Carpenter, T. Murphy and M. J. Smylie, *Changing patterns in electroweak precision with new color-charged states: Oblique corrections and the W boson mass*, [2204.08546](#).
- [19] M. Du, Z. Liu and P. Nath, *CDF W mass anomaly in a Stueckelberg extended standard model*, [2204.09024](#).
- [20] M. E. Peskin and T. Takeuchi, *A New constraint on a strongly interacting Higgs sector*, *Phys. Rev. Lett.* **65** (1990) 964–967.
- [21] W. J. Marciano and J. L. Rosner, *Atomic parity violation as a probe of new physics*, *Phys. Rev. Lett.* **65** (1990) 2963–2966.
- [22] D. C. Kennedy and P. Langacker, *Precision electroweak experiments and heavy physics: A Global analysis*, *Phys. Rev. Lett.* **65** (1990) 2967–2970.
- [23] Y.-Z. Fan, T.-P. Tang, Y.-L. S. Tsai and L. Wu, *Inert Higgs Dark Matter for New CDF W-boson Mass and Detection Prospects*, [2204.03693](#).
- [24] C.-R. Zhu, M.-Y. Cui, Z.-Q. Xia, Z.-H. Yu, X. Huang, Q. Yuan et al., *GeV antiproton/gamma-ray excesses and the W-boson mass anomaly: three faces of $\sim 60 - 70$ GeV dark matter particle?*, [2204.03767](#).
- [25] B.-Y. Zhu, S. Li, J.-G. Cheng, R.-L. Li and Y.-F. Liang, *Using gamma-ray observation of dwarf spheroidal galaxy to test a dark matter model that can interpret the W-boson mass*

- anomaly, [2204.04688](#).
- [26] H. Song, W. Su and M. Zhang, *Electroweak Phase Transition in 2HDM under Higgs, Z-pole, and W precision measurements*, [2204.05085](#).
- [27] H. Bahl, J. Braathen and G. Weiglein, *New physics effects on the W-boson mass from a doublet extension of the SM Higgs sector*, [2204.05269](#).
- [28] Y. Heo, D.-W. Jung and J. S. Lee, *Impact of the CDF W-mass anomaly on two Higgs doublet model*, [2204.05728](#).
- [29] K. S. Babu, S. Jana and V. P. K., *Correlating W-Boson Mass Shift with Muon $g - 2$ in the 2HDM*, [2204.05303](#).
- [30] T. Biekötter, S. Heinemeyer and G. Weiglein, *Excesses in the low-mass Higgs-boson search and the W-boson mass measurement*, [2204.05975](#).
- [31] Y. H. Ahn, S. K. Kang and R. Ramos, *Implications of New CDF-II W Boson Mass on Two Higgs Doublet Model*, [2204.06485](#).
- [32] X.-F. Han, F. Wang, L. Wang, J. M. Yang and Y. Zhang, *A joint explanation of W-mass and muon $g-2$ in 2HDM*, [2204.06505](#).
- [33] G. Arcadi and A. Djouadi, *The 2HD+a model for a combined explanation of the possible excesses in the CDF M_W measurement and $(g - 2)_\mu$ with Dark Matter*, [2204.08406](#).
- [34] K. Ghorbani and P. Ghorbani, *W-Boson Mass Anomaly from Scale Invariant 2HDM*, [2204.09001](#).
- [35] Y. Cheng, X.-G. He, Z.-L. Huang and M.-W. Li, *Type-II Seesaw Triplet Scalar and Its VEV Effects on Neutrino Trident Scattering and W mass*, [2204.05031](#).
- [36] X. K. Du, Z. Li, F. Wang and Y. K. Zhang, *Explaining The New CDFII W-Boson Mass In The Georgi-Machacek Extension Models*, [2204.05760](#).
- [37] S. Kanemura and K. Yagyu, *Implication of the W boson mass anomaly at CDF II in the Higgs triplet model with a mass difference*, [2204.07511](#).
- [38] P. Mondal, *Enhancement of the W boson mass in the Georgi-Machacek model*, [2204.07844](#).
- [39] D. Borah, S. Mahapatra, D. Nanda and N. Sahu, *Type II Dirac Seesaw with Observable ΔN_{eff} in the light of W-mass Anomaly*, [2204.08266](#).
- [40] J. M. Yang and Y. Zhang, *Low energy SUSY confronted with new measurements of W-boson mass and muon $g-2$* , [2204.04202](#).
- [41] X. K. Du, Z. Li, F. Wang and Y. K. Zhang, *Explaining The Muon $g - 2$ Anomaly and New CDF II W-Boson Mass in the Framework of (Extra)Ordinary Gauge Mediation*, [2204.04286](#).
- [42] T.-P. Tang, M. Abdughani, L. Feng, Y.-L. S. Tsai and Y.-Z. Fan, *NMSSM neutralino dark matter for W-boson mass and muon $g - 2$ and the promising prospect of direct detection*, [2204.04356](#).
- [43] P. Athron, M. Bach, D. H. J. Jacob, W. Kotlarski, D. Stöckinger and A. Voigt, *Precise calculation of the W boson pole mass beyond the Standard Model with FlexibleSUSY*, [2204.05285](#).
- [44] M.-D. Zheng, F.-Z. Chen and H.-H. Zhang, *The $W\ell\nu$ -vertex corrections to W-boson mass in*

- the R-parity violating MSSM*, [2204.06541](#).
- [45] A. Ghoshal, N. Okada, S. Okada, D. Raut, Q. Shafi and A. Thapa, *Type III seesaw with R-parity violation in light of m_W (CDF)*, [2204.07138](#).
- [46] P. Athron, A. Fowlie, C.-T. Lu, L. Wu, Y. Wu and B. Zhu, *The W boson Mass and Muon $g - 2$: Hadronic Uncertainties or New Physics?*, [2204.03996](#).
- [47] K. Cheung, W.-Y. Keung and P.-Y. Tseng, *Iso-doublet Vector Leptoquark solution to the Muon $g - 2$, R_{K,K^*} , R_{D,D^*} , and W-mass Anomalies*, [2204.05942](#).
- [48] A. Bhaskar, A. A. Madathil, T. Mandal and S. Mitra, *Combined explanation of W-mass, muon $g - 2$, $R_{K^{(*)}}$ and $R_{D^{(*)}}$ anomalies in a singlet-triplet scalar leptoquark model*, [2204.09031](#).
- [49] M. Blennow, P. Coloma, E. Fernández-Martínez and M. González-López, *Right-handed neutrinos and the CDF II anomaly*, [2204.04559](#).
- [50] F. Arias-Aragón, E. Fernández-Martínez, M. González-López and L. Merlo, *Dynamical Minimal Flavour Violating Inverse Seesaw*, [2204.04672](#).
- [51] X. Liu, S.-Y. Guo, B. Zhu and Y. Li, *Unifying gravitational waves with W boson, FIMP dark matter, and Majorana Seesaw mechanism*, [2204.04834](#).
- [52] T. A. Chowdhury, J. Heeck, S. Saad and A. Thapa, *W boson mass shift and muon magnetic moment in the Zee model*, [2204.08390](#).
- [53] O. Popov and R. Srivastava, *The Triplet Dirac Seesaw in the View of the Recent CDF-II W Mass Anomaly*, [2204.08568](#).
- [54] H. M. Lee and K. Yamashita, *A Model of Vector-like Leptons for the Muon $g - 2$ and the W Boson Mass*, [2204.05024](#).
- [55] J. Kawamura, S. Okawa and Y. Omura, *W boson mass and muon $g - 2$ in a lepton portal dark matter model*, [2204.07022](#).
- [56] A. Crivellin, M. Kirk, T. Kitahara and F. Mescia, *Correlating $t \rightarrow cZ$ to the W Mass and B Physics with Vector-Like Quarks*, [2204.05962](#).
- [57] K. I. Nagao, T. Nomura and H. Okada, *A model explaining the new CDF II W boson mass linking to muon $g - 2$ and dark matter*, [2204.07411](#).
- [58] E. Bagnaschi, J. Ellis, M. Madigan, K. Mimasu, V. Sanz and T. You, *SMEFT Analysis of m_W* , [2204.05260](#).
- [59] L. Di Luzio, R. Gröber and P. Paradisi, *Higgs physics confronts the M_W anomaly*, [2204.05284](#).
- [60] V. Cirigliano, W. Dekens, J. de Vries, E. Mereghetti and T. Tong, *Beta-decay implications for the W-boson mass anomaly*, [2204.08440](#).
- [61] G.-W. Yuan, L. Zu, L. Feng and Y.-F. Cai, *W-boson mass anomaly: probing the models of axion-like particle, dark photon and Chameleon dark energy*, [2204.04183](#).
- [62] G. Cacciapaglia and F. Sannino, *The W boson mass weighs in on the non-standard Higgs*, [2204.04514](#).
- [63] K. Sakurai, F. Takahashi and W. Yin, *Singlet extensions and W boson mass in the light of the CDF II result*, [2204.04770](#).
- [64] J. J. Heckman, *Extra W-Boson Mass from a D3-Brane*, [2204.05302](#).

- [65] N. V. Krasnikov, *Nonlocal generalization of the SM as an explanation of recent CDF result*, [2204.06327](#).
- [66] Z. Péli and Z. Trócsányi, *Vacuum stability and scalar masses in the superweak extension of the standard model*, [2204.07100](#).
- [67] P. F. Perez, H. H. Patel and A. D. Plascencia, *On the W-mass and New Higgs Bosons*, [2204.07144](#).
- [68] R. A. Wilson, *A toy model for the W/Z mass ratio*, [2204.07970](#).
- [69] K.-Y. Zhang and W.-Z. Feng, *Explaining W boson mass anomaly and dark matter with a U(1) dark sector*, [2204.08067](#).
- [70] MUON G-2 collaboration, B. Abi et al., *Measurement of the Positive Muon Anomalous Magnetic Moment to 0.46 ppm*, *Phys. Rev. Lett.* **126** (2021) 141801, [[2104.03281](#)].
- [71] A. Arbey, F. Mahmoudi, O. Stal and T. Stefaniak, *Status of the Charged Higgs Boson in Two Higgs Doublet Models*, *Eur. Phys. J. C* **78** (2018) 182, [[1706.07414](#)].
- [72] M. Misiak and M. Steinhauser, *Weak radiative decays of the B meson and bounds on M_{H^\pm} in the Two-Higgs-Doublet Model*, *Eur. Phys. J. C* **77** (2017) 201, [[1702.04571](#)].
- [73] G. C. Branco, P. M. Ferreira, L. Lavoura, M. N. Rebelo, M. Sher and J. P. Silva, *Theory and phenomenology of two-Higgs-doublet models*, *Phys. Rept.* **516** (2012) 1–102, [[1106.0034](#)].
- [74] S. L. Glashow and S. Weinberg, *Natural Conservation Laws for Neutral Currents*, *Phys. Rev. D* **15** (1977) 1958.
- [75] E. A. Paschos, *Diagonal Neutral Currents*, *Phys. Rev. D* **15** (1977) 1966.
- [76] J. Song and Y. W. Yoon, *$W\gamma$ decay of the elusive charged Higgs boson in the two-Higgs-doublet model with vectorlike fermions*, *Phys. Rev. D* **100** (2019) 055006, [[1904.06521](#)].
- [77] D. Eriksson, J. Rathsmann and O. Stal, *2HDMC: Two-Higgs-Doublet Model Calculator Physics and Manual*, *Comput. Phys. Commun.* **181** (2010) 189–205, [[0902.0851](#)].
- [78] P. Bechtle, S. Heinemeyer, T. Klingl, T. Stefaniak, G. Weiglein and J. Wittbrodt, *HiggsSignals-2: Probing new physics with precision Higgs measurements in the LHC 13 TeV era*, *Eur. Phys. J. C* **81** (2021) 145, [[2012.09197](#)].
- [79] P. Bechtle, D. Dercks, S. Heinemeyer, T. Klingl, T. Stefaniak, G. Weiglein et al., *HiggsBounds-5: Testing Higgs Sectors in the LHC 13 TeV Era*, *Eur. Phys. J. C* **80** (2020) 1211, [[2006.06007](#)].
- [80] D. Das and I. Saha, *Search for a stable alignment limit in two-Higgs-doublet models*, *Phys. Rev. D* **91** (2015) 095024, [[1503.02135](#)].
- [81] ATLAS collaboration, G. Aad et al., *Combined measurements of Higgs boson production and decay using up to 80 fb^{-1} of proton-proton collision data at $\sqrt{s} = 13$ TeV collected with the ATLAS experiment*, *Phys. Rev. D* **101** (2020) 012002, [[1909.02845](#)].
- [82] I. P. Ivanov, *Minkowski space structure of the Higgs potential in 2HDM*, *Phys. Rev. D* **75** (2007) 035001, [[hep-ph/0609018](#)].
- [83] S. Kanemura, T. Kubota and E. Takasugi, *Lee-Quigg-Thacker bounds for Higgs boson masses in a two doublet model*, *Phys. Lett. B* **313** (1993) 155–160, [[hep-ph/9303263](#)].

- [84] A. G. Akeroyd, A. Arhrib and E.-M. Naimi, *Note on tree level unitarity in the general two Higgs doublet model*, *Phys. Lett. B* **490** (2000) 119–124, [[hep-ph/0006035](#)].
- [85] S. Chang, S. K. Kang, J.-P. Lee and J. Song, *Higgs potential and hidden light Higgs scenario in two Higgs doublet models*, *Phys. Rev. D* **92** (2015) 075023, [[1507.03618](#)].
- [86] A. Barroso, P. M. Ferreira, I. P. Ivanov and R. Santos, *Metastability bounds on the two Higgs doublet model*, *JHEP* **06** (2013) 045, [[1303.5098](#)].
- [87] HFLAV collaboration, Y. S. Amhis et al., *Averages of b -hadron, c -hadron, and τ -lepton properties as of 2018*, *Eur. Phys. J. C* **81** (2021) 226, [[1909.12524](#)].
- [88] H.-J. He, N. Polonsky and S.-f. Su, *Extra families, Higgs spectrum and oblique corrections*, *Phys. Rev. D* **64** (2001) 053004, [[hep-ph/0102144](#)].
- [89] W. Grimus, L. Lavoura, O. M. Ogreid and P. Osland, *The Oblique parameters in multi-Higgs-doublet models*, *Nucl. Phys. B* **801** (2008) 81–96, [[0802.4353](#)].
- [90] PARTICLE DATA GROUP collaboration, P. A. Zyla et al., *Review of Particle Physics*, *PTEP* **2020** (2020) 083C01.
- [91] T. P. Cheng, E. Eichten and L.-F. Li, *Higgs Phenomena in Asymptotically Free Gauge Theories*, *Phys. Rev. D* **9** (1974) 2259.
- [92] H. Komatsu, *Behavior of the Yukawa and the Quartic Scalar Couplings in Grand Unified Theories*, *Prog. Theor. Phys.* **67** (1982) 1177.
- [93] P. Basler, P. M. Ferreira, M. Mühlleitner and R. Santos, *High scale impact in alignment and decoupling in two-Higgs doublet models*, *Phys. Rev. D* **97** (2018) 095024, [[1710.10410](#)].
- [94] J. Oredsson, *2HDME : Two-Higgs-Doublet Model Evolver*, *Comput. Phys. Commun.* **244** (2019) 409–426, [[1811.08215](#)].
- [95] ATLAS collaboration, M. Aaboud et al., *Search for Higgs bosons produced via vector-boson fusion and decaying into bottom quark pairs in $\sqrt{s} = 13$ TeV pp collisions with the ATLAS detector*, *Phys. Rev. D* **98** (2018) 052003, [[1807.08639](#)].
- [96] ATLAS collaboration, M. Aaboud et al., *Measurements of gluon-gluon fusion and vector-boson fusion Higgs boson production cross-sections in the $H \rightarrow WW^* \rightarrow e\nu\mu\nu$ decay channel in pp collisions at $\sqrt{s} = 13$ TeV with the ATLAS detector*, *Phys. Lett. B* **789** (2019) 508–529, [[1808.09054](#)].
- [97] ATLAS collaboration, M. Aaboud et al., *Cross-section measurements of the Higgs boson decaying into a pair of τ -leptons in proton-proton collisions at $\sqrt{s} = 13$ TeV with the ATLAS detector*, *Phys. Rev. D* **99** (2019) 072001, [[1811.08856](#)].
- [98] ATLAS collaboration, G. Aad et al., *Higgs boson production cross-section measurements and their EFT interpretation in the 4ℓ decay channel at $\sqrt{s} = 13$ TeV with the ATLAS detector*, *Eur. Phys. J. C* **80** (2020) 957, [[2004.03447](#)].
- [99] CMS collaboration, A. M. Sirunyan et al., *Search for $t\bar{t}H$ production in the $H \rightarrow b\bar{b}$ decay channel with leptonic $t\bar{t}$ decays in proton-proton collisions at $\sqrt{s} = 13$ TeV*, *JHEP* **03** (2019) 026, [[1804.03682](#)].
- [100] CMS collaboration, A. M. Sirunyan et al., *Search for the Higgs boson decaying to two muons in*

- proton-proton collisions at $\sqrt{s} = 13$ TeV*, *Phys. Rev. Lett.* **122** (2019) 021801, [1807.06325].
- [101] CMS collaboration, *Measurements of properties of the Higgs boson in the four-lepton final state in proton-proton collisions at $\sqrt{s} = 13$ TeV*, .
- [102] CMS collaboration, *Measurements of differential Higgs boson production cross sections in the leptonic WW decay mode at $\sqrt{s} = 13$ TeV*, .
- [103] K. Cheung, A. Jueid, J. Kim, S. Lee, C.-T. Lu and J. Song, *Comprehensive study of the light charged Higgs boson in the type-I two-Higgs-doublet model*, 2201.06890.
- [104] ATLAS collaboration, M. Aaboud et al., *Search for charged Higgs bosons decaying via $H^\pm \rightarrow \tau^\pm \nu_\tau$ in the τ +jets and τ +lepton final states with 36 fb^{-1} of pp collision data recorded at $\sqrt{s} = 13$ TeV with the ATLAS experiment*, *JHEP* **09** (2018) 139, [1807.07915].
- [105] CMS collaboration, A. M. Sirunyan et al., *Search for a heavy pseudoscalar boson decaying to a Z and a Higgs boson at $\sqrt{s} = 13$ TeV*, *Eur. Phys. J. C* **79** (2019) 564, [1903.00941].
- [106] ATLAS collaboration, *Search for heavy resonances decaying into a Z boson and a Higgs boson in final states with leptons and b-jets in 139 fb^{-1} of pp collisions at $\sqrt{s} = 13 \text{ TeV}$ with the ATLAS detector*, .
- [107] ATLAS collaboration, G. Aad et al., *Search for heavy Higgs bosons decaying into two tau leptons with the ATLAS detector using pp collisions at $\sqrt{s} = 13$ TeV*, *Phys. Rev. Lett.* **125** (2020) 051801, [2002.12223].
- [108] M. Misiak, A. Rehman and M. Steinhauser, *Towards $\bar{B} \rightarrow X_s \gamma$ at the NNLO in QCD without interpolation in m_c* , *JHEP* **06** (2020) 175, [2002.01548].